Archives of Virology (2023) 168:132
https://doi.org/10.1007/s00705-023-05766-x

ORIGINAL ARTICLE

Phospholipid analysis of two influenza A virus-infected cell lines differing in their viral replication kinetics

Kohei Kawabata[1] · Yuichiro Sato[1] · Takanori Kubo[1] · Akira Tokumura[1] · Hiroyuki Nishi[1] · Kinjiro Morimoto[1]

Received: 12 February 2023 / Accepted: 17 March 2023 / Published online: 7 April 2023

Abstract

Fluctuations in phospholipid composition in infected cells during influenza A virus replication were analyzed using two different susceptible host cell lines: H292 cells, exhibiting a rapid cytopathic effect, and A549 cells, exhibiting a retarded cytopathic effect. Microarray analysis demonstrated that A549 cells recognized influenza A virus invasion, expression of pathogen recognition genes was affected, and antiviral genes were activated. On the other hand, H292 cells did not display such an antiviral state, and in these cells, rapid virus amplification and a rapid cytopathic effect were observed. Levels of ceramide, diacylglycerol, and lysolipids were higher in virus-infected cells than in the corresponding mock-infected cells at the later stages of infection. The accumulation of these lipids in IAV-infected cells occurred together with viral replication. The relationship between the characteristic features of ceramide, diacylglycerol, and lysolipid in the plasma membrane, where enveloped viruses are released, and their role in viral envelope formation are discussed. Our results indicate that viral replication disturbs cellular lipid metabolism, with consequences for viral replication kinetics.

Introduction

Influenza A virus (IAV), a member of the family *Orthomyxoviridae*, is a negative-sense, single-stranded, segmented RNA virus [1]. IAV is classified into subtypes based on variations in the viral hemagglutinin (HA) and neuraminidase (NA), which are membrane glycoproteins that are present in the virion envelope [2]. IAV circulates and causes seasonal epidemics of disease and is known to have caused pandemics. Every year, there are an estimated 1 billion cases of IAV infection globally, of which 3 to 5 million are severe, resulting in 290,000 to 650,000 influenza-related deaths [3].

The IAV virion binds to a specific receptor on the host cell, and the viral RNA genome invades the cytoplasm by uncoating of the nucleocapsid. The viral genome is then amplified for replication and transcription, and viral proteins are produced using the translational machinery of the host cell. These viral proteins and nucleocapsids containing genomic RNA assemble into virions, and the progeny virions acquire a host-derived lipid envelope during budding at the plasma membrane [2]. Viral infection induces different types of cellular responses in different cell types, resulting in increased production of factors that participate in the virus recognition mechanism, cytokine production, including interferon production, and regulation of cellular metabolism, including lipid metabolism [4–7].

The entry of virions into host cells starts with attachment at the cell surface, where the assembly and release of progeny virions also occur. The plasma membrane, which separates the cell from the outside environment, is composed of a lipid bilayer made up of phospholipids and cholesterol and contains various glycoproteins and glycolipids. IAV uses sialic acid on glycoproteins and glycolipids as an entry receptor. The plasma membrane, which interacts with the outside environment, is involved in a variety of cellular processes such as the transport of materials, ion conductivity, cell signaling, cell adhesion, endocytosis, and exocytosis. [7, 8]. Most of the phospholipids in the lipid bilayer are present in one of six major glycerophospholipid types: phosphatidic acid (PA), phosphatidylcholine (PC), phosphatidylethanolamine (PE), phosphatidylglycerol (PG), phosphatidylinositol (PI), phosphatidylserine (PS), and sphingomyelin (SM) [8, 9]. Generally, PC is the major component of most mammalian cell membranes, whereas PE is the most abundant in purified virions [10]. The phospholipid composition of the

Handling Editor: William G Dundon.

✉ Kinjiro Morimoto
mori-k@yasuda-u.ac.jp

[1] Faculty of Pharmacy, Yasuda Women's University, 6-13-1, Yasuhigashi, Asaminamiku, Hiroshima 731-0153, Japan

host cell depends on the host species and differs between mock-infected and virus-infected cells and also differs from that of virions produced from these cells. There are also differences in lipid composition between IAV strains [10].

IAV acquires its host-derived envelope during the budding of progeny virions. At the budding site, there is a change in the phospholipid content of microdomains within the host plasma membrane. Elevated sphingolipid turnover and altered lipid composition of plasma membranes of infected cells have been reported in infections with various viruses [11], including human immunodeficiency virus [12], flaviviruses [13], coronaviruses [14], IAV [15], vesicular stomatitis virus [16], and rotaviruses [17]. Structures referred to as "lipid rafts" are sites of assembly and budding of various enveloped viruses as well as sites of viral binding and entry [18, 19]. However, a convergent view of the role of lipid metabolic pathways during influenza virus replication is lacking, particularly the pathways that are required for the generation of the viral envelope, and their contribution to virus pathogenicity is not well understood [20, 21]. Understanding the effect of phospholipid metabolism on viral pathogenesis will provide important insights that will aid in the development of therapeutic strategies against microbial infections [22].

In the present study, we examined changes in the lipid composition of the host plasma membrane at various stages of IAV infection, using cells differing in IAV replication kinetics. Major phospholipid classes in IAV- and mock-infected cells were quantified by lipidomic analysis and compared at different stages of virus infection. Altered phospholipid metabolism, which is a hallmark of influenza virus infection *in vitro* and *in vivo*, is of interest as a unique pathogenicity-dependent signature for influenza virus. Here, we focused on changes in the content in ceramides (CERs) during virus amplification. It is known that CER accumulation in the inner leaflet of the plasma membrane favors blebbing and membrane evagination [21, 22, 24]. The interplay between CER and IAV has not yet been fully elucidated, and results of this study raise the question of a potential role for CER during IAV infection.

Materials and methods

Virus and cells

A stock of influenza A/H3N2/Udorn/72 virus was used for virus infection. The virus strain was grown in the chorioallantonic fluid of 10-day-old chicken eggs. Aliquots of the virus preparation were stored at -80°C until use. Human lung carcinoma A549 cells (ATCC CCL185) and H292 cells (NCI-H292, ATCC CRL1848) were used as host cells. Both cell lines are fully permissive for influenza A virus infection. These cells were grown in RPMI-1640 medium supplemented with 10% fetal bovine serum and 100 IU of penicillin and 100 µg of streptomycin (GIBCO, NY, USA) per mL.

Virus infection

A549 or H292 cells were infected with the A/H3N2/Udorn/72 strain at a multiplicity of infection (MOI) of 3. The virus titer (focus-forming units [ffu]/mL) was determined using a fluorescent focus assay. After 1 h of adsorption, the cells were washed with phosphate-buffered saline (PBS) and incubated in serum-free RPMI-1640 medium under 5% CO_2 at 37°C. At 4, 8, 12, and 24 h postinfection (hpi), infected cells were prepared for subsequent experiments.

Direct immunofluorescence and staining of virus-infected cells

Virus-infected cells were fixed with 80% acetone at 8 hpi and stained with a diluted fluorescein isothiocyanate (FITC)-conjugated monoclonal antibody against the influenza A virus nucleoprotein (NP) (D67J; Pierce-Antibodies, MA, USA). Images were taken under a fluorescence microscope (Olympus CKX41, Tokyo, Japan) at 400x magnification. For cell staining, the cells were fixed with 80% acetone and stained with 0.5% amido black 10 B (Wako Pure Chemical Corporation, Tokyo, Japan) in 45% ethanol and 10% acetic acid as described previously [25, 26].

Microarray analysis of virus-infected cells

A549 or H292 cells were infected with the A/H3N2/Udorn/72 strain at an MOI of 3. At 4 and 8 hpi, total RNA was extracted from the virus-infected cells and the corresponding mock-infected cells using an RNeasy Kit (QIAGEN Inc., CA, USA). A portion of the RNA preparation was subjected to analysis using Agilent Expression Array Sure Print G3 Human Gene Expression 8 × 60k ver. 2 (Agilent Technologies, CA, USA). The expression levels of mRNAs were analyzed using approximately 50,000 probes, allowing full coverage of the human transcriptome. Using this analysis with our RNA preparations, positive signals were obtained with 7,681 and 7,924 probes in mock- or IAV-infected A549 cells and H292 cells, respectively (Supplementary Data 1). The expression levels of different genes were compared between IAV-infected and mock-infected cells.

Liquid chromatography–tandem mass spectrometry (LC-MS/MS) analysis

A549 and H292 cells infected with IAV or mock-infected cells in 12-well culture plates were incubated for the

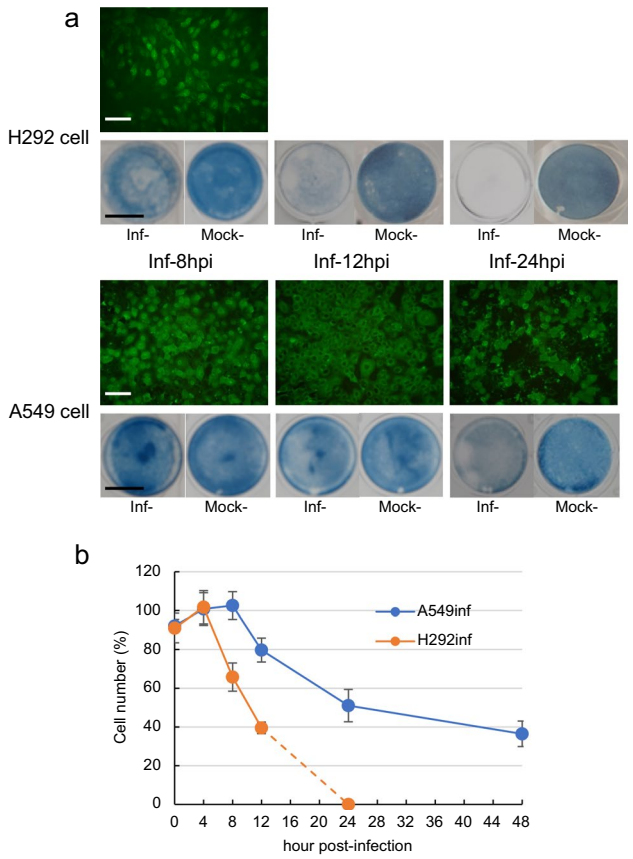

Fig. 1 (a) CPE due to IAV infection and (b) number of cells remaining on the culture plate. IAV-infected H292 and A549 cells were stained with FITC-conjugated anti-NP antibody or 0.5% amido black at 8, 12, and 24 hpi. White scale bars, 100 μm; black scale bars, 5 mm. H292 cells were counted at 4, 8, and 12 hpi, and A549 cells were counted at 4, 8,12, 24, and 48 hpi. The percentages are in comparison to mock-infected cells.

indicated times. After removal of the supernatant, the resident cells were washed with PBS and detached by treatment with 500 μL of 0.25% trypsin containing 1 mM EDTA. Four hundred microliters of the cell suspension was added to 600 μL of distilled water, as well as 10 μL of a mixture of internal standard for LC-MS/MS analysis containing standard lysolipids and diacyllipids (as shown in Supplementary Data 2) and 3.7 mL of a chloroform-methanol mixture (1:2, v/v). The mixed preparations were subjected to phase separation by adding 1.25 mL each of chloroform and distilled water acidified to pH 2–2.5, essentially as described by Bligh and Dyer [27]. The chloroform phase was withdrawn and evaporated, the residue was redissolved in 1 mL of mobile phase, and 50 μL of 5 mM EDTA was added. Levels of individual molecular species of lipids tested are tentatively shown as pmol/10^3 cells based on peak ratios to the corresponding internal standard. Total levels of each lipid class were calculated semi-quantitatively as the sum of those of the individual molecular species. The rest (100 μL) of the cell suspension was used to count the cells.

The lipid profile of each cell preparation was determined using an LC-MS/MS system composed of an LC-20AD pump, SIL-20AC auto-sampler, CBM-20A system controller, DGU-20A5R degasser, CTO-20A column oven, FCV-20AH2 valve unit, and LCMS-8040 MS system equipped with ESI as the ionization source (Shimadzu Corp., Kyoto, Japan). The entire system was operated using LabSolutions software. The analytical column was a Mastro2 C18 column (2.0 × 150 mm; particle size, 5.0 μm; Shimadzu Corp.). The column was kept at 45°C during analysis. The mobile phase consisted of a methanol-water mixture (95:5, v/v) containing 5 mM ammonium formate. Isocratic separation was achieved using this mobile phase. The flow rate was maintained at 0.2 and 0.4 mL/min for the analysis of lysolipids and diacyllipids, respectively. The injection volume was in the range of 5–40 μL. MS/MS parameters of each lysolipid and diacyllipid are shown in Supplementary Data 2.

Real-time fluorescent quantitative PCR

A549 or H292 cells (10^5 cells/well in 48-well plates) were infected with the A/H3N2/Udorn/72 strain at an MOI of 3. At 8 and 12 hpi (both cell lines), and at 24 and 48 hpi (only A549 cells only), total RNA was extracted from the infected cells using a Luna Cell Ready Lysis Module (New England Biolabs Inc., MA, USA). Some of the RNAs were analyzed using a Luna Cell Ready One-Step RT-qPCR Kit (New England Biolabs Inc., MA, USA) using the primers FLUAM-7F (CTTCTAACCGAGGTCGAAACGTA), FLUAM-161-R (GGTGACAGGATTGGTCTTGTCTTTA), and FLUAM-49-P6 (FAM-TCAGGCCCCCTCAAAGCCGAG-BHQ1) [28]. Briefly, the reverse transcription step was carried out at 55°C for 10 min, followed by heat denaturation at 95°C for 1 min. The qPCR step consisted of 45 cycles of 95°C for 10 s and 60°C for 30 s. The qPCR was performed using a Thermal Cycler Dice Real Time System III (Takara, Japan). The value obtained for the threshold cycle (Ct) was adjusted for cell number in the corresponding culture and expressed as a relative amount of viral RNA.

Statistical analysis

The results are expressed as the mean ± standard deviation (SD). Data were analyzed using JMP® 14.2 statistical software (SAS Institute, Cary, North Carolina, USA). The statistical significance of the differences among groups was analyzed using Student's *t*-test. $P < 0.05$ (shown as *) or $P < 0.01$ (shown as **) were considered significant.

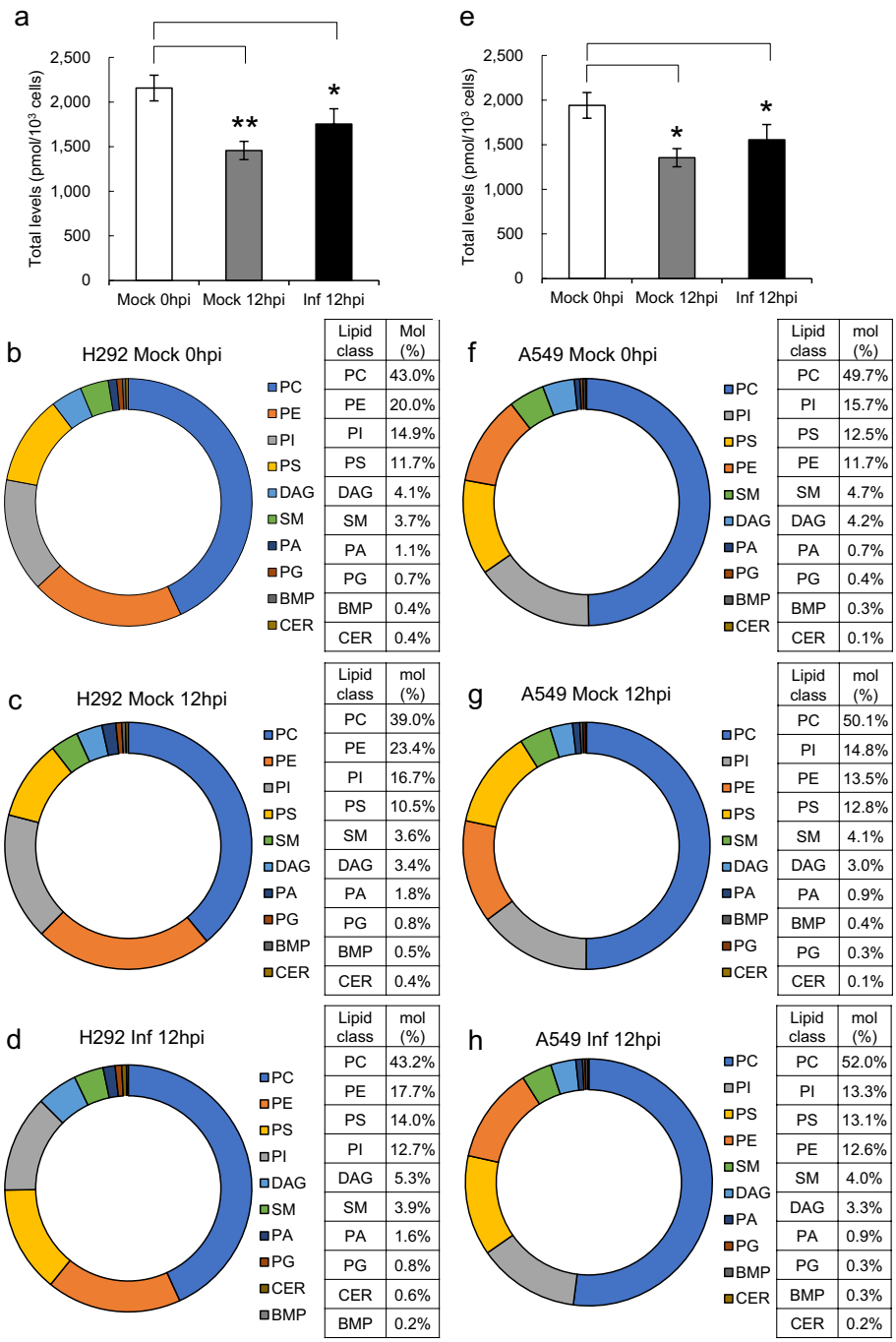

Fig. 2 Total diacyllipid content in mock- and IAV-infected H292 and A549 cells (a, e) and the phospholipid composition of H292 and A549 cells (b-d, f-h). The total diacyllipid content was determined in mock-infected cells at 0 hpi and in mock- and IAV-infected cells at 12 hpi. The molar percentage of each major glycerolipid and sphingolipid class is shown (b-d, f-h).

Results and discussion

We performed a comparative lipid analysis with two cell lines that differ in their sensitivity to influenza virus infection, with H292 cells exhibiting a stronger cytopathic effect (CPE) than A549 cells. Immunofluorescence microscopy showed that both cell lines were infected to a similar extent by IAV. At 12 hpi, more than half of the H292 cells had detached from the culture plate, and at 24 hpi, almost all of the cells had detached. On the other hand, most of the A549 cells remained attached to the culture plate at 12 hpi (Fig. 1a). The number of attached cells on the culture plate decreased as the virus infection progressed, and the rate was faster for H292 cells than for A549 cells (Fig. 1b).

We also investigated how the kinetics of virus replication may be corelated with fluctuations in the lipid composition of the cells. IAV- and mock-infected H292 or A549 cells at 0, 4, 8, and 12 hpi were subjected to lipid profile analysis (Supplementary Data 3). The total lipid content per cell number (pmol/10^3 cells) in mock-infected cells was

Table 1 Comparison of diacyllipids in IAV- and mock-infected H292 and A549 cells at 12 hpi

	H292					A549				
		Mean[a]	SD[b]	Inf/Mock[c]	*P*-value[d]		Mean	SD	Inf	*P*-value/Mock
PC	Mock	568.6	50.7	**1.33**	0.014	Mock	678.1	54.0	1.19	0.138
	Inf	757.0	58.3		*	Inf	809.0	99.9		
PE	Mock	340.2	22.7	0.91	0.283	Mock	182.3	4.6	**1.07**	0.027
	Inf	309.6	34.9			Inf	195.6	5.0		*
PG	Mock	11.1	0.9	**1.33**	0.032	Mock	4.6	0.1	1.17	0.052
	Inf	14.8	1.5		*	Inf	5.4	0.3		
PI	Mock	242.6	22.1	0.92	0.486	Mock	199.9	8.4	1.04	0.266
	Inf	222.7	38.0			Inf	207.2	3.0		
PS	Mock	152.5	8.1	**1.61**	0.041	Mock	173.8	3.0	**1.18**	0.003
	Inf	245.1	35.8		*	Inf	204.4	5.7		**
PA	Mock	26.4	3.2	1.05	0.647	Mock	12.7	0.7	1.06	0.508
	Inf	27.7	2.8			Inf	13.5	1.6		
BMP	Mock	7.4	0.5	**0.55**	0.013	Mock	5.6	0.9	0.93	0.465
	Inf	4.1	1.0		*	Inf	5.2	0.3		
DAG	Mock	49.6	6.7	**1.89**	0.006	Mock	40.0	3.0	**1.28**	0.009
	Inf	93.8	1.5		**	Inf	51.2	2.6		**
SM	Mock	53.2	4.0	**1.28**	0.032	Mock	55.9	0.9	**1.10**	0.012
	Inf	67.9	6.1		*	Inf	61.6	1.6		*
CER	Mock	5.1	0.5	**2.18**	0.007	Mock	1.7	0.1	1.41	0.085
	Inf	11.1	1.2		**	Inf	2.4	0.4		
Total	Mock	1456.7	102.3	1.20	0.075	Mock	1354.6	38.5	1.15	0.065
	Inf	1753.8	171.5			Inf	1555.3	103.7		

[a]Mean (pmol/10^3 cells), [b]SD (standard deviation), [c]Inf/Mock at 12 hpi (the number of virus-infected cells divided by the number of mock-infected cells), [d]Significant differences in the number (as shown in bold type) of virus-infected cells compared to the number of mock-infected cells are indicated as follows: *, $P < 0.05$; **, $P < 0.01$.

determined at 0 h and 12 h, and in IAV-infected cells it was determined at 12 hpi (Fig. 2a and e). At 12 hpi, the total lipid content was reduced in both mock- and IAV-infected cultures. The total activity of the lipid degradation pathway surpassed that of the lipid synthetic pathway because of the lack of a lipid supply when serum-free medium was used. In addition, the total amount of diacyllipid was slightly reduced in the infected cells (Fig. 2a and e).

The diacylphospholipid composition varies among different types of cells, and that of virions differs from that of the infected cells from which they produced [10]. This suggests that virus replication might alter the lipid profile of the cell. The profiles of the major diacyl phospholipids in mock- and virus-infected cells are shown in Fig. 2b and f. PC is the major component in most mammalian cell membranes [9, 10]. PC was found to be abundant in both cells lines, but the relative amount of PE was found to be higher in H292 cells. PI accounts for roughly 15% and PS accounts for roughly 10% of total phospholipids, with minor differences. The relative abundance of the different lipids was PC > PE > PI > PS in H292 cells and PC > PI > PE = PS in A549 cells. Diacylglycerol (DAG) comprised 3–5% of the total lipids. Of the minor phospholipid classes, PG, PA, and bis-(monoacylglycerol)-phosphatidic acid (BMP) represented less than 1% of the total lipid content.

Sphingolipids, another phospholipid subfamily, were also analyzed. SM is the most abundant member of this subfamily [9, 29] and was found to constitute 3.5–4.5% of the total lipid content in both cell lines. SM is more abundant in A549 cells than in H292 cells. CER, which is a central intermediate in sphingolipid metabolism and plays an important role as a secondary messenger in diverse cell signaling pathways, accounts for less than 1% of the lipid in these cells and is more abundant in H292 cells than in A549 cells. Although glycerophospholipids are sufficient to form membrane bilayers by themselves, less-abundant lipid species, especially sphingolipids, play an important role in determining the biophysical and biological properties of lipid bilayers. For example, a particular type of microdomain, called a lipid raft, is enriched in cholesterol and sphingolipids and plays a role in many biological processes, including numerous signal transduction pathways, apoptosis, and protein sorting during both exocytosis and endocytosis, as well as being

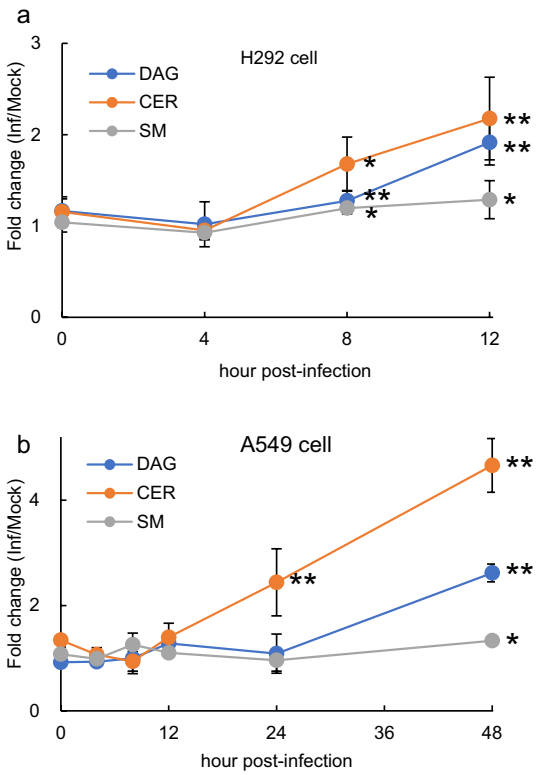

Fig. 3 Changes in the DAG, CER, and SM content of IAV-infected H292 or A549 cells. The relative amounts of DAG, CER, and SM in IAV-infected cells compared to those in mock-infected cells were determined at 0, 4, 8, and 12 hpi for H292 cells (a) and at 0, 4, 8, 12, 24, and 48 hpi for A549 cells (b). Significant differences between virus-infected cells and mock-infected cells are indicated as follows: *, $P < 0.05$; **, $P < 0.01$.

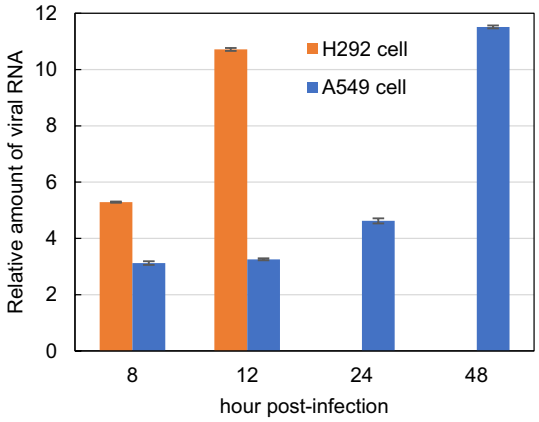

Fig. 4 Quantitation of viral RNA by real-time RT-PCR. The relative amount of viral RNA in the cells (equivalent to 10^5 cells) was calculated using the Ct values obtained from H292 cells at 8 and 12 hpi and A549 cells at 8, 12, 24, and 48 hpi.

responsible for virus entry and viral assembly and release [18, 23].

Viral infection can disturb many cellular metabolic processes that are associated with lipid metabolism. We found that the proportions of the major phospholipid classes changed somewhat as IAV infection progressed. A difference in the overall phospholipid composition of mock-infected and IAV-infected cells was observed in both H292 (Fig. 2b-d) and A549 cells (Fig. 2f-h), but the relative amounts of the major glycerophospholipid classes did not show a marked difference during infection in either cell type.

The effect of IAV on lipid composition was evaluated by comparing the content of individual phospholipid classes in IAV-infected and mock-infected cells at 12 hpi (Table 1), and the relative amounts of PC, PG, PS, DAG, SM, and CER were found to be increased by viral infection in H292 cells. Among the major glycerophospholipids, the largest change was observed for PS (1.61-fold). Interestingly, a 1.89-fold higher level of DAG was found in IAV-infected cells when compared to mock-infected cells. DAG is a central and important lipid in glycerophospholipid metabolism and acts as a second messenger, activating protein kinase C in the signal transduction pathway. SM is the most abundant membrane sphingolipid, representing 3.5–4.0% of the total lipid content (Fig. 2b-d). The relative amount of SM was 1.28-fold higher in IAV-infected cells than in mock-infected cells. Although the total amount of CER was much less than that of SM, the relative content of CER in IAV-infected cells compared to that in mock-infected cells was 2.18-fold higher (Table 1). Sphingolipids are known to be responsible for blebbing and curvature or evagination of the plasma membrane, where assembly and release of IAV occurs.

In A549 cells, which are less sensitive to IAV infection and exhibit a slower development of CPE, the relative change in lipid composition due to infection was less pronounced than in H292 cells. DAG (1.28-fold) and CER (1.41-fold) increased at 12 hpi.

A time-course analysis was performed to examine changes in the amounts of sphingolipids and DAG in H292 cells at 4, 8, and 12 hpi, and DAG and CER were found to significantly increase with time postinfection (Fig. 3a). In A549 cells, a similar effect was observed, but not until later time points (24 and 48 hpi), which correlated with the slower progression of CPE in A549 cells (Fig. 3b). The SM content did not change significantly in either cell type.

To investigate changes in the amount of viral RNA in infected cells, real-time RT-PCR analysis was performed (Fig. 4). Total viral RNA (viral genome and messenger sense RNA) was examined at 8 and 12 hpi in both cell lines and at 24 and 48 hpi in A549 cells. Viral RNA amplification

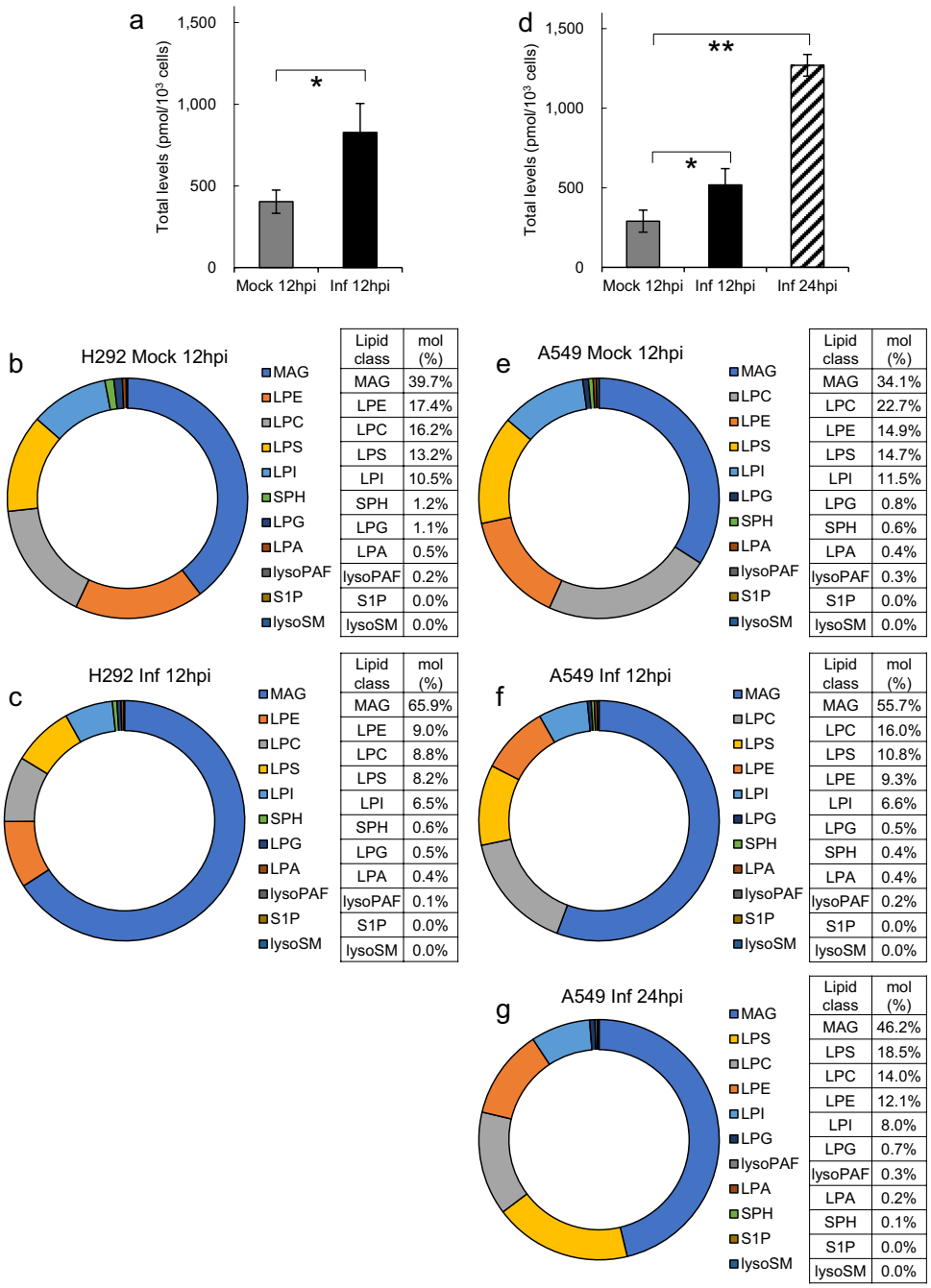

Lipid class	mol (%)
MAG	39.7%
LPE	17.4%
LPC	16.2%
LPS	13.2%
LPI	10.5%
SPH	1.2%
LPG	1.1%
LPA	0.5%
lysoPAF	0.2%
S1P	0.0%
lysoSM	0.0%

Lipid class	mol (%)
MAG	34.1%
LPC	22.7%
LPE	14.9%
LPS	14.7%
LPI	11.5%
LPG	0.8%
SPH	0.6%
LPA	0.4%
lysoPAF	0.3%
S1P	0.0%
lysoSM	0.0%

Lipid class	mol (%)
MAG	65.9%
LPE	9.0%
LPC	8.8%
LPS	8.2%
LPI	6.5%
SPH	0.6%
LPG	0.5%
LPA	0.4%
lysoPAF	0.1%
S1P	0.0%
lysoSM	0.0%

Lipid class	mol (%)
MAG	55.7%
LPC	16.0%
LPS	10.8%
LPE	9.3%
LPI	6.6%
LPG	0.5%
SPH	0.4%
LPA	0.4%
lysoPAF	0.2%
S1P	0.0%
lysoSM	0.0%

Lipid class	mol (%)
MAG	46.2%
LPS	18.5%
LPC	14.0%
LPE	12.1%
LPI	8.0%
LPG	0.7%
lysoPAF	0.3%
LPA	0.2%
SPH	0.1%
S1P	0.0%
lysoSM	0.0%

Fig. 5 Total lysolipid content in mock- and IAV-infected H292 and A549 cells (a, d) and the lysolipid composition in H292 and A549 cells (b-c, e-g). The total lysolipid content was measured in mock-infected cells at 12 hpi and in IAV-infected cells at 12 and 24 hpi. The major lysolipid classes are shown as a molar percentage (b-c, e-g).

was found to be delayed in A549 cells compared to H292 cells, which correlated with the delayed cell death seen in Fig.1. H292 cells produced 1.6×10^7 ffu of progeny virus at per mL 24 hpi, and A549 cells produced 5.4×10^6 ffu/mL at 24 hpi.

Taken together, our results suggest that viral replication brings about changes in phospholipid metabolism. The relative amounts of CER and DAG in IAV-infected cells increased with time, although their effect on the total phospholipid content was small. DAG is a central lipid of glycerophospholipid metabolism. Therefore, we believe it is produced by increased degradation of glycerophospholipids due to viral infection. CER is a central intermediate in sphingolipid metabolism. CER, which has a cone-shaped structure, influences membrane curvature and fluidity, leading to positive curvature of the plasma membrane [23, 24]. Therefore, the increase in CER would favor budding of virions. We suggest that CER might also be an indicator molecule of cellular dysfunction and cell death.

Virus infection affects total lysophospholipid content. In H292 cells, the total amount of lysophospholipid at 12 hpi was higher than in mock-infected cells (Fig. 5a). In A549 cells, the total amount of lysophospholipids was increased

Table 2 Number of genes with expression levels that were altered by at least 4-fold during IAV infection

H292 cells	4 hpi	8 hpi	4 hpi or 8 hpi	4 hpi and 8 hpi
Total	99	131	181	49
Upregulated	44	28	68	4
Downregulated	55	103	113	45
A549 cells				
Total	157	311	426	42
Upregulated	113	251	346	18
Downregulated	44	60	80	24

mRNA levels were compared between IAV-infected and mock-infected cells using microarray analysis (Supplementary Data 1).

at 12 hpi, and the increase became more prominent at later times in proportion to virus replication (Fig. 5d).

The generation of lysolipids could be related to the degradation of diacyllipids, which might disturb the structure and dynamics of the cell plasma membrane. The amount of the lysolipid monoacylglycerol (MAG) in H292 cells increased from 39.7% in mock-infected cells to 65.9% in IAV-infected cells at 12 hpi (Fig. 5b-c). In A549 cells, a similar increase in MAG was detected (34.1% in mock-infected cells versus 55.7% at 12 hpi and 46.2% at 24 hpi in IAV-infected cells; Fig. 5e-g). The generation of MAG could be caused by the degradation of lysophospholipids, which are degradation products of diacylphospholipids. Alternatively, MAG is produced from DAG by diacylglycerol lipase. The increase in DAG levels in IAV-infected cells, as shown in Fig. 3, would contribute to the increase in MAG levels. This degradation is commonly caused by virus infection [12], which disturbs lipid metabolism via generation of lysolipids by phospholipases and lipases. Another important role of lysophospholipids is to promote positive curvature by introducing inverted cone-shaped molecules into the membrane [10]. Like CER, lysophospholipids might promote virus production by disturbing the membrane structure.

H292 and A549 cells exhibit differences in their sensitivity to IAV infection, which could be observed in comparative gene expression analysis. Microarray analysis showed that 7,681 genes were significantly expressed in IAV-infected and mock-infected A549 cells and that 7,924 genes were expressed in H292 cells (Supplementary Data 1). As shown in Table 2, in A549 cells, 346 genes were upregulated by more than 4-fold at 4 or 8 hpi as compared to those in mock-infected cells, and 80 genes were downregulated by less than 4-fold. A total of 426 genes showed changes in expression levels at the early stages of IAV infection.

In H292 cells, the expression of 181 genes was affected by IAV infection, 113 of which were downregulated and 68 of which were upregulated. Both cell lines showed altered profiles of gene expression in the early stages of IAV infection. A549 cells, exhibiting retarded CPE, displayed increased expression of many genes. In H292 cells, which are more sensitive to IAV infection, the number of genes with altered expression was lower and the number of upregulated genes was smaller than the number of downregulated ones.

We then focused on genes related to pathogen recognition and sensing of viral infection, which provide the first line of protection against invading pathogens acting either to eliminate the pathogen or to maintain tolerance [4]. In particular, the expression levels of virus-recognition genes, including Toll-like receptors (TLRs), retinoic acid-inducible gene I (RIG-I)-like receptors (RLRs), and nucleotide-binding oligomerization domain (NOD)-like receptors (NLRs), were examined during the early stages of IAV infection (Table 3). In A549 cells, the TLR3, MYD88, TRIM21,

Table 3 Genes related to pathogen recognition with altered levels of expression during IAV infection

Gene	Description	H292		A549		Accession no.
		4 hpi	8 hpi	4 hpi	8 hpi	
	TLRs					
TLR3	Toll-like receptor 3	0.34	0.62	0.17	**4.15**	NM_003265
MYD88	Myeloid differentiation primary response gene 88	0.31	0.83	0.36	**2.48**	NM_002468
	RLRs					
TRIM21	Tripartite motif containing 21	0.02	1.77	0.72	**3.74**	NM_003141
RIG-I (DDX58)	DEAD (Asp-Glu-Ala-Asp) box polypeptide 58	0.26	1.02	1.05	**4.62**	NM_014314
MAVS	Mitochondrial antiviral signaling protein	**-3.05**	**-2.74**	0.08	0.13	NM_020746
	NLRs					
NLRC5	NLR family, CARD domain containing 5	0.18	0.08	0.44	**3.91**	NM_032206
NOD2	Nucleotide-binding oligomerization domain containing 2	0.17	0.50	-0.08	**2.61**	NM_022162

Changes in gene expression of 4-fold or more (shown as $\log_2$ values), as indicated by microarray analysis (Supplementary Data 1), are shown in bold. mRNA expression levels were compared between IAV-infected cells and their corresponding mock-infected cells at 4 and 8 hpi.

RIG-I, NLRC5, and NOD2 genes were strongly upregulated at 8 hpi. In H292 cells, expression of these genes was lower, and the expression of the MAVS gene, which contributes to antiviral innate immunity, was prominently downregulated. These genes are activated early in infection and are critical for influenza virus cytopathogenesis. Pathogen-recognition receptors activate specific signaling pathways that lead to the expression of genes related to production of type I interferons (IFNs) and inflammatory cytokines and trigger apoptosis. In this study, genes encoding interferon regulatory factors, Jak/Stat signaling factors, and IFNs (especially, IFN–λs), as well as interferon-inducible genes, including MX1, MX2, and 2'-5'-oligoadenylate synthetase 1, 2, and 3, were upregulated in IAV-infected A549 cells at 8 hpi, but most of these genes were not significantly affected by IAV infection in H292 cells (Supplementary Data 4 and 5). These responses to IAV infection in A549 cells may serve as a cellular defense mechanism to reduce potential cytotoxic effects.

In conclusion, IAV infection alters cellular homeostasis, disturbs the overall metabolic state of the cell, and can ultimately result in cell death. The mechanism by which this occurs is likely to depend on the cell type. Viruses can induce cell death through apoptosis, necrosis, necroptosis, and pyroptosis, but the mechanisms involved are not completely understood [30–35]. In this study, we used cells that differ in their sensitivity to IAV infection. A549 cells can recognize the invasion of pathogens and induce an antiviral state or express interferon-related genes [6] (Table 2, Supplementary Data 4). H292 cells do not recognize IAV, and therefore, virus replication, disturbance of cellular metabolism, and cell death occur more rapidly in these cells. We found that replication of the virus and disturbance of phospholipid metabolism (with a relative increase in CER, DAG, and lysolipids) occurred simultaneously. Lipid metabolism is involved in various cellular physiological states [9]. Expression of genes encoding enzymes involved in phospholipid metabolism, including sphingomyelinase, ceramide synthetase, and diacylglycerol lipase, did not change significantly in the early stage of virus replication (Supplementary Data 6), but the relative levels of CER and MAG increased with time as IAV infection progressed. These lipids can have a significant effect on the dynamics of the plasma membrane, where envelope IAV particles assemble and bud. Previous studies have shown that ceramide is associated with different pathobiological disorders, such as cancer, liver disease, diabetes, cardiovascular disease, and lung inflammation [7, 36–41]. Ceramide can also enhance or inhibit viral replication, suggesting that clinical manipulation of ceramide metabolism might be a potential strategy for combating viral infections [11, 24, 42]. Further investigations are required to gain a better understanding of the role of lipids in the molecular pathogenesis of IAV, which might be useful for the development new therapeutic strategies.

Supplementary Information The online version contains supplementary material available at https://doi.org/10.1007/s00705-023-05766-x.

Acknowledgements The authors are grateful for access to the Cooperative Research Center of Yasuda Women's University.

Author contributions KK, AT, HN, and KM conceived and designed the study. KK, TK, and KM conducted the experiments. KK, YS, AT, HN, and KM analyzed the data and wrote the original draft. All authors have reviewed and approve the final manuscript.

Funding This work was supported in part by a grant from Yasuda Women's University.

Data availability Data availability statement The datasets generated during the current study are available from the corresponding author on reasonable request.

Declarations

Conflict of interest The authors declare that they have no competing interests.

References

1. ICTV (International Committee on Taxonomy of Viruses) https://ictv.global/report_9th/RNAneg/Orthomyxoviridae
2. Palese P, Shaw ML (2007) *Orthomyxoviridae*: the viruses and their replication. In: Knipe DM, Howley PM et al (eds) Fields virology, 5th edn. Wolters Kluwer Health/Lippincott Williams & Wilkins, Philadelphia, pp 1647–1689
3. WHO, Influenza (seasonal) fact sheet, https://www.who.int/news-room/fact-sheets/detail/influenza-(seasonal)
4. Kawai T, Akira S (2009) The roles of TLRs, RLRs and NLRs in pathogen recognition. Int Immunol 21(4):317–337. https://doi.org/10.1093/intimm/dxp017
5. Majdoul S, Compton AA (2021) Lessons in self-defence: inhibition of virus entry by intrinsic immunity. Nat Rev Immunol 22(6):339–352. https://doi.org/10.1038/s41577-021-00626-8
6. Samuel CE (2001) Antiviral actions of interferons. Clin Microbiol Rev 14(4):778–809. https://doi.org/10.1128/CMR.14.4.778-809.2001
7. Hannun YA, Obeid LM (2018) Sphingolipids and their metabolism in physiology and disease. Nat Rev Mol Cell Biol 19(3):175–191. https://doi.org/10.1038/nrm.2017.107
8. Hermansson M, Hokynar K, Somerharju P (2011) Mechanisms of glycerophospholipid homeostasis in mammalian cells. Prog Lipid Res 50(3):240–257. https://doi.org/10.1016/j.plipres.2011.02.004
9. Cockcroft S (2021) Mammalian lipids: structure, synthesis and function. Essays Biochem 65(5):813–845. https://doi.org/10.1042/EBC20200067
10. Ivanova PT, Myers DS, Milne SB, McClaren JL, Thomas PG, Brown HA (2015) Lipid composition of viral envelope of three strains of influenza virus—not all viruses are created equal. ACS Infect Dis 1(9):399–452. https://doi.org/10.1021/acsinfecdis.5b00040
11. Beckmann N, Becker KA (2021) Ceramide and related molecules in viral infections. Int J Mol Sci 22(11):5676. https://doi.org/10.3390/ijms22115676

12. Haughey NJ, Cutler RG, Tamara A, McArthur JC, Vargas DL, Pardo CA, Turchan J, Nath A, Mattson MP (2004) Perturbation of sphingolipid metabolism and ceramide production in HIV-dementia. Ann Neurol 55(2):257–267. https://doi.org/10.1002/ana.10828
13. Martín-Acebes MA, Merino-Ramos T, Blázquez TAB, Casas J, Escribano-Romero E, Sobrino F, Saiz JC (2014) The composition of West Nile virus lipid envelope unveils a role of sphingolipid metabolism in flavivirus biogenesis. J Virol 88(20):12041–12054. https://doi.org/10.1128/JVI.02061-14
14. Yan B, Chu H, Yang D, Sze KH, Lai PM, Yuan S, Shuai H, Wang Y, Kao RYT, Chan JFW, Yuen KY (2019) Characterization of the lipidomic profile of human coronavirus-infected cells: implications for lipid metabolism remodeling upon coronavirus replication. Viruses 11(1):73. https://doi.org/10.3390/v11010073
15. Zhou Y, Pu J, Wu Y (2021) The role of lipid metabolism in influenza a virus infection. Pathogens 10(3):303. https://doi.org/10.3390/pathogens10030303
16. Havranek KE, Ballista JMR, Hines KM, Brindley MA (2021) Untargeted lipidomics of vesicular stomatitis virus-infected cells and viral particles. Viruses 14(1):3. https://doi.org/10.3390/v14010003
17. Gaunt ER, Zhang Q, Cheung W, Wakelam MJO, Lever AML, Desselberger U (2013) Lipidome analysis of rotavirus-infected cells confirms the close interaction of lipid droplets with viroplasms. J Gen Virol 94(7):1576–1586. https://doi.org/10.1099/vir.0.049635-0
18. Munro S (2003) Lipid rafts: elusive or illusive? Cell 115(4):377–388. https://doi.org/10.1016/s0092-8674(03)00882-1
19. Avota E, Bodem J, Chithelen J, Mandasari P, Beyersdorf N, Schneider-Schaulies J (2021) The manifold roles of sphingolipids in viral infections. Front Physiol 12:715527. https://doi.org/10.3389/fphys.2021.71552
20. Tanner LB, Chng C, Guan XL, Lei Z, Rozen SG, Wenk MR (2014) Lipidomics identifies a requirement for peroxisomal function during influenza virus replication. J Lipid Res 55(7):1357–1365. https://doi.org/10.1194/jlr.M049148
21. Audi A, Soudani N, Dbaibo G, Zaraket H (2020) Depletion of host and viral sphingomyelin impairs influenza virus infection. Front Microbiol 11:612. https://doi.org/10.3389/fmicb.2020.00612
22. Monson EA, Helbig KJ (2021) Host upregulation of lipid droplets drives antiviral responses. Cell Stress 5(9):143–145. https://doi.org/10.15698/cst2021.09.256
23. Verderio C, Gabrielli M, Giussani P (2018) Role of sphingolipids in the biogenesis and biological activity of extracellular vesicles. J Lipid Res 59(8):1325–1340. https://doi.org/10.1194/jlr.R083915
24. Soudani N, Hage-Sleiman R, Karam W, Dbaibo G, Zaraket H (2019) Ceramide suppresses influenza A virus replication in vitro. J Virol 93(7):e00053-e119. https://doi.org/10.1128/JVI.00053-19
25. Morimoto K, Sato Y (2016) Anti-influenza virus activity of high-mannose binding lectins derived from genus *Pseudomonas*. Virus Res 223:64–72. https://doi.org/10.1016/j.virusres.2016.06.020
26. Matoba Y, Sato Y, Oda K, Hatori Y, Morimoto K (2021) Lectins engineered to favor a glycan-binding conformation have enhanced antiviral activity. J Biol Chem 296:100698. https://doi.org/10.1016/j.jbc.2021.100698
27. Bligh EG, Dyer WJA (1959) Rapid method of total lipid extraction and purification. Can J Biochem Physiol 37(8):911–917
28. WHO information for the molecular detection of influenza viruses, Annex 2A: real-time RT-PCR protocols
29. Slotte JP (2013) Biological functions of sphingomyelins. Prog Lipid Res 52(4):424–437. https://doi.org/10.1016/j.plipres.2013.05.001
30. Brydon EWA, Morris SJ, Sweet C (2005) Role of apoptosis and cytokines in influenza virus morbidity. FEMS Microbiol Rev 29(4):837–850. https://doi.org/10.1016/j.femsre.2004.12.003
31. Herold S, Ludwig S, Pleschka S, Wolff T (2012) Apoptosis signaling in influenza virus propagation, innate host defense, and lung injury. J Leukoc Biol 92(1):75–82. https://doi.org/10.1189/jlb.1011530
32. Tran AT, Cortens JP, Du Q, Wilkins JA, Coombs KM (2013) Influenza virus induces apoptosis via BAD-mediated mitochondrial dysregulation. J Virol 87(2):1049–1060. https://doi.org/10.1128/JVI.02017-12
33. Danthi P (2016) Viruses and the diversity of cell death. Annu Rev Virol 3(1):533–553. https://doi.org/10.1146/annurev-virology-110615-042435
34. Atkin-Smith GK, Duan M, Chen W, Poon IKH (2018) The induction and consequences of Influenza A virus-induced cell death. Cell Death Dis 9(10):1002. https://doi.org/10.1038/s41419-018-1035-6
35. Imre G (2020) Cell death signalling in virus infection. Cell Signal 76:109772. https://doi.org/10.1016/j.cellsig.2020.109772
36. Galadari S, Rahman A, Pallichankandy S, Galadari A, Thayyullathil F (2013) Role of ceramide in diabetes mellitus: evidence and mechanisms. Lipids Health Dis 12:98. https://doi.org/10.1186/1476-511X-12-98
37. Kasumov T, Li L, Li M, Gulshan K, Kirwan JP, Liu X, Previs S, Willard B, Smith JD, McCullough A (2015) Ceramide as a mediator of non-alcoholic fatty liver disease and associated atherosclerosis. PLoS ONE 10:e0126910. https://doi.org/10.1371/journal.pone.0126910
38. Galadari S, Rahman A, Pallichankandy S, Thayyullathil F (2015) Tumor suppressive functions of ceramide: evidence and mechanisms. Apoptosis 20(5):689–711. https://doi.org/10.1007/s10495-015-1109-1
39. Laaksonen R, Ekroos K, Sysi-Aho M, Hilvo M, Vihervaara T, Kauhanen D, Suoniemi M, Hurme R, März W, Scharnagl H, Stojakovic T, Vlachopoulou E, Lokki M-L, Nieminen MS, Klingenberg R, Matter CM, Hornemann T, Jüni P, Rodondi N, Räber L, Windecker S, Gencer B, Pedersen ER, Tell GS, Nygård O, Mach F, Sinisalo J, Lüscher TF (2016) Plasma ceramides predict cardiovascular death in patients with stable coronary artery disease and acute coronary syndromes beyond LDL-cholesterol. Eur Heart J 37:1967–1976. https://doi.org/10.1093/eurheartj/ehw148
40. Becker KA, Riethmüller J, Zhang Y, Gulbins E (2010) The role of sphingolipids and ceramide in pulmonary inflammation in cystic fibrosis. Open Respir Med J 4:39–47. https://doi.org/10.2174/1874306401004020039
41. Tam VC, Quehenberger O, Oshansky CM, Suen R, Armando AM, Treuting PM, Thomas PG, Dennis EA, Aderem A (2013) Lipidomic profiling of influenza infection identifies mediators that induce and resolve inflammation. Cell 154(1):213–227. https://doi.org/10.1016/j.cell.2013.05.052
42. Seo YJ, Blake C, Alexander S, Hahm B (2010) Sphingosine 1-phosphate-metabolizing enzymes control influenza virus propagation and viral cytopathogenicity. J Virol 84(16):8124–8131. https://doi.org/10.1128/JVI.00510-10